JACS
JOURNAL OF THE AMERICAN CHEMICAL SOCIETY
pubs.acs.org/JACS
Article

Water Poisons H_2 Activation at the Au–TiO_2 Interface by Slowing Proton and Electron Transfer between Au and Titania

K. B. Sravan Kumar,[§] Todd N. Whittaker,[§] Christine Peterson, Lars C. Grabow, and Bert D. Chandler*

Cite This: J. Am. Chem. Soc. 2020, 142, 5760–5772
Read Online

ABSTRACT: Understanding the dynamic changes at the active site during catalysis is a fundamental challenge that promises to improve catalytic properties. While performing Arrhenius studies during H_2 oxidation over Au/TiO_2 catalysts, we found different apparent activation energies (E_{app}) depending on the feedwater pressure. This is partially attributed to changing numbers of metal–support interface (MSI) sites as water coverage changes with temperature. Constant water coverage studies showed two kinetic regimes: fast heterolytic H_2 activation directly at the MSI (E_{app} ~ 25 kJ/mol) and significantly slower heterolytic H_2 activation mediated by water (E_{app} ~ 45 kJ/mol). The two regimes had significantly different kinetics, suggesting a complicated mechanism of water poisoning. Density functional theory (DFT) showed water has minor effects on the reaction thermodynamics, primarily attributable to intrinsic differences in surface reactivity of different Au sites in the DFT model. The DFT model suggested significant surface restructuring of the TiO_2 support during heterolytic H_2 adsorption; evidence for this phenomenon was observed during *in situ* infrared spectroscopy experiments. A monolayer of water on the hydroxylated TiO_2 surface increased the H_2 dissociation activation barrier by ~0.2 eV, in good agreement the difference in experimentally measured values. DFT calculations suggested H_2 activation goes through a proton-coupled electron-transfer-like mechanism. During proton transfer to a basic support hydroxyl group, electron density is distributed through the gold nanorod and partially localized on the protonated support hydroxyl group. Water slows H_2 activation by slowing this H^+ transfer, forcing negative charge buildup on the Au and increasing the transition state energy.

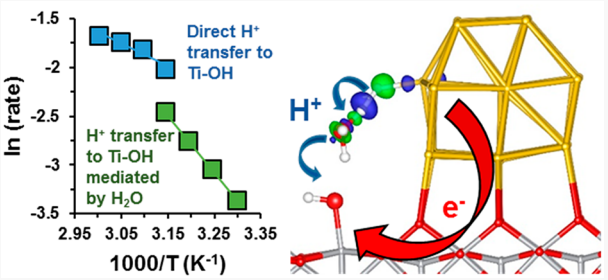

INTRODUCTION

Supported metal catalysts, typically consisting of a metal nanoparticle immobilized on an oxide support, are mainstays of the petrochemical and environmental remediation industries.[1] The interface between the metal nanoparticle and the oxide support is often considered the active site for many industrially important reactions, including CO_2 hydrogenation,[2−5] methanol synthesis,[6] biomass upgrading,[7] CO oxidation,[8−10] the water–gas shift reaction,[11,12] nitroarene hydrogenation,[13,14] and electrocatalytic energy conversion.[15,16] In spite of the commercial importance of these materials, developing an understanding of the nature of the catalytic active site, and the factors that influence catalyst activity at the metal–support interface, remain significant challenges.

The interplay between metal, support, and adsorbates is therefore an area of widespread interest; our understanding of the complex chemistries involved continues to evolve.[17,18] Charge transfer between the two components may occur in either direction depending on the metal, the reducibility of the support, the exposed metal facets, and the presence of defects.[19−26] Reaction intermediates can bridge the two phases,[10] and reactions can occur between species on each phase.[9,27] Reactive species can also be transferred from one phase to the other, as is the case of hydrogen spillover.[28,29] Finally, active sites at or near the interface can dynamically respond to the reaction environment,[30,31] experience poisoning or blocking by strongly adsorbing species, or deactivate over extended periods of time.[32,33]

We are working to better understand the complexity associated with reactivity at the metal–support interface (MSI) using the relatively simple, yet industrially important hydrogen oxidation reaction over supported Au catalysts. More than 95% of industrial H_2 is generated through hydrocarbon steam reforming and water–gas shift reactions, which produces an ~1% CO impurity. The preferential oxidation of CO (PrOx) is a potential means of removing this CO cheaply and cleanly, but the reaction places large performance demands on the catalyst.[34−37] Au nanoparticles are exceptional CO oxidation catalysts[8,38,39] and have excellent selectivity in

Received: December 20, 2019
Published: February 21, 2020

https://dx.doi.org/10.1021/jacs.9b13729
J. Am. Chem. Soc. 2020, 142, 5760–5772

PrOx when an optimal amount of physisorbed H_2O is present.[40]

Water can have a significant effect on catalytic performance, particularly in selective oxidation reactions, where the role of water varies.[41] Ertl and co-workers concluded that water preferentially adsorbs at coordinatively unsaturated (cus) Ru sites, poisoning CO oxidation over RuO_2 catalysts.[42] Conversely, Haruta and Daté,[43] as well as others,[8,38,44,45] demonstrated water promotion of CO oxidation catalysis over supported Au at low pressures. Both the Behm and Mullins groups have shown that water can change the reaction mechanism of CO oxidation on Au/TiO_2.[46,47] While it is clear that adsorbed water can profoundly affect catalytic systems, the origins of this effect are not well understood and appear to vary from system to system.

We recently showed that water poisons H_2 activation over Au, which takes place at the MSI via heterolytic H_2 dissociation.[48] This finding was surprising given that most metals bind H_2 through dissociative chemisorption. Heterolytic activation of nonacidic bonds such as H−H and C−H bonds has been claimed in some solid systems, but these systems typically require clever modifications to yield strong Frustrated Lewis Pairs (FLPs).[49−58]

The goals of this study are to elucidate the origins of the water poisoning effects and to understand the driving force behind the heterolytic H_2 activation. In particular, we examine the conclusion that water blocks the most reactive MSI sites and more deeply probe the details of heterolytic H_2 activation at the MSI. We find that the poisoning, and indeed the nature of the active site, is far more dynamic than a simple "site-blocking" mechanism suggests. Additionally, we show the Au/TiO_2 catalysts have an intimate electronic interaction that allows for the rapid exchange of both protons and electrons between the two components. This exchange is also tied to structural changes on the support surface. Thus, water poisons the reaction not by simply blocking the active site, but by interfering in the ability of the MSI to distribute these charges in the H_2 activation transition state.

RESULTS AND DISCUSSION

Constant P_{H_2O} Arrhenius Studies. We initially concluded the loss of activity with increased water coverage resulted from losing the most active H_2 activation sites at the metal−support interface.[48] Arrhenius studies carried out with 9 and 19 Torr water in the feed yielded two different apparent activation barriers: 50 ± 3 and 76 ± 12 kJ/mol, respectively (see the Supporting Information). The feedwater content should not affect a "true" activation barrier; further, these values are considerably larger than the E_{app} values Haruta and co-workers reported for H_2−D_2 equilibration over Au/TiO_2 (36 kJ/mol).[59] Given that both reactions occur at the MSI, and both are considered to be H_2 activation limited, the measured apparent activation energies ought to be reasonably similar. We also found the reaction kinetics varied substantially with the feed P_{H_2O} (*vida infra*). Collectively, these data indicate the water-poisoning chemistry is more complex and more interesting than simple "site blocking" of the most active H_2 dissociation sites.

Calculated Elementary Step Energetics for H_2 Oxidation. We previously showed homolytic activation of H_2 on Au−Au sites is thermodynamically and kinetically less favorable than heterolytic activation at the MSI.[48] The homolytic pathway is unlikely to be affected by the water layer, beyond water's ability to cover the more reactive surfaces. We therefore focus our analysis on the (faster) heterolytic H_2 activation at Au MSI sites and Au metal−water interface (MWI) sites.

The various reaction sites in the computational model are described briefly here; full details are available in the Supporting Information. A $TiO_2(110)$ surface models the support and gold is modeled as a nanorod with different facets. As Scheme 1 shows, the left side of the nanorod truncates in the Au(111) surface, while the right side truncates in a Au(211) step edge; Miller indices associated with individual surface atoms are also included. The $TiO_2(110)$ surface was fully hydroxylated with water, leading to two chemically distinct surface hydroxyl groups in close proximity to the Au nanorod: (i) hydroxyl groups bound to coordinatively unsaturated Ti sites (HO_{cus}) and (ii) hydroxyl groups resulting from protonation of bridging O atoms (HO_{br}). The former are Brønsted bases; the latter have Brønsted acidity. Both Ti−OH sites alternate along the length of the Au nanorod such that both hydroxyls are accessible to adsorbates on the Au.

Scheme 1. Schematic Representation of the Au/TiO_2 Computational Model Showing the Metal−Support Interface and Metal-Water Interface Sites[a]

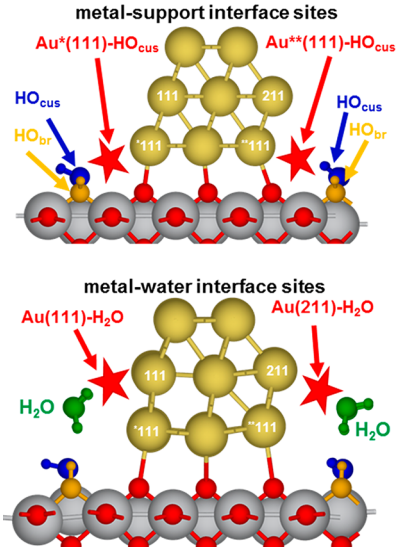

[a]The Au*(111)−HO_{cus} and Au**(111)−HO_{cus} sites are indicated on the left side and right sides of the top portion of the scheme, respectively. The metal−water interface is described by the Au(111)−H_2O and Au(211)−H_2O sites on the left side and right sides of the bottom portion of the scheme. Further details on the computational model can be found in the Materials and Methods section in the Supporting Information.

Our model is designed to describe reactivity at the MSI in the presence and absence of water, where metal, support, and Brønsted acid−base chemistry can all be explored. Each potential reaction site is chemically distinct. Reactivity on the Au nanorod, away from the MSI, is described simply with the atoms involved (e.g., dissociative H_2 chemisorption on Au(211)−Au(211) sites is faster than that on Au(111)−Au(111) sites).[48] Both sides of the model have Au(111) atoms interacting with the support, but the Au(111) structure is truncated and replaced by interactions with the support O

https://dx.doi.org/10.1021/jacs.9b13729
J. Am. Chem. Soc. 2020, 142, 5760−5772

Table 1. Elementary Step Energetics for H_2 Oxidation at the MSI without Water and at the MWI with Water[a]

key H_2 oxidation elementary steps with and without H_2O at the interface				
entry	reaction site/reactant	reaction	E_a (eV)	ΔE (eV)
O_2 activation				
ES1	Au*(111)−HO_{br} (MSI)	Au + O_2 + HO_{br} → Au^{2+}−^{-}OOH + $^{-}O_{br}$	0.05	−0.49
ES2	Au(211)−H_2O−HO_{br} (MWI)	Au + O_2 + HO_{br} → Au^{2+}−^{-}OOH + $^{-}O_{br}$	0.48	−0.39
ES3	Au(211)−H_2O−$^{+}H_2O_{cus}$ (MWI)	Au + O_2 + $^{+}H_2O_{cus}$ → Au^{2+}−^{-}OOH + HO_{cus}	0.19	−0.52
Au−OOH protonation				
ES4	Au*(111)−$^{+}H_2O_{cus}$ (MSI)	Au^{2+}−^{-}OOH + $^{+}H_2O_{cus}$ → Au^{2+}−H_2O_2 + HO_{cus}	0.04	−0.27
ES5	Au(211)−H_2O−$^{+}H_2O_{cus}$ (MWI)	Au^{2+}−^{-}OOH $^{+}H_2O_{cus}{}^{+}$ → Au^{2+}−H_2O_2 + HO_{cus}	0.19	−0.55
Au−H_2O_2 protonation				
ES6	Au*(111)−$^{+}H_2O_{cus}$ (MSI)	Au^{2+}−H_2O_2 + Au + $^{+}H_2O_{cus}$ →Au^{+}−OH + Au^{2+}−H_2O + HO_{cus}	0.41	−1.81
ES7	Au(211)−H_2O−$^{+}H_2O_{cus}$ (MWI)	Au^{2+}−H_2O_2 + Au + $^{+}H_2O_{cus}$ →Au^{+}−OH + Au^{2+}−H_2O + HO_{cus}	0.37	−2.11
Au−OH protonation				
ES8	Au*(111)−$^{+}H_2O_{cus}$ (MSI)	Au^{+}−OH + $^{+}H_2O_{cus}$ → Au^{2+}−H_2O + HO_{cus}	0.00	−1.17
ES9	Au(211)−H_2O−$^{+}H_2O_{cus}$ (MWI)	Au^{+}−OH + $^{+}H_2O_{cus}$ → Au^{2+}−H_2O + HO_{cus}	0.13	−0.70
Au−O protonation				
ES10	$^{+}H_2O_{cus}$ (MSI)	Au−O + $^{+}H_2O_{cus}$ → Au^{+}−OH + HO_{cus}	0.16	−1.04
ES11	Au(211)−H_2O−$^{+}H_2O_{cus}$ (MWI)	Au−O + $^{+}H_2O_{cus}$ → Au^{+}−OH + HO_{cus}	0.02	−0.63
Au−H deprotonation				
ES12	Au*(111)−HO_{cus} (MSI)	Au−H^{-} + HO_{cus}→ Au^{2-} + $^{+}H_2O_{cus}$	0.39	−0.73
ES13	Au(211)−H_2O−HO_{cus} (MWI)	Au−H^{-} + HO_{cus}→ Au^{2-} + $^{+}H_2O_{cus}$	0.55	−0.71
proton exchange				
ES14	HO_{cus}, HO_{br} (MSI)	HO_{br} + HO_{cus}→ $^{-}O_{br}$ + $^{+}H_2O_{cus}$	0.49	0.08
ES15	HO_{cus}, HO_{br} (MWI)	HO_{br} + HO_{cus}→ $^{-}O_{br}$ + $^{+}H_2O_{cus}$	0.44	0.00

[a]Elementary steps at the MSI were published previously.[48]

atoms. We define the combination of metal and support at this site as "Au*(111)−HO_{cus}". The "*" (asterisk) indicates direct interaction with the support (and consequent lower Au coordination); the "HO_{cus}" indicates the close proximity of the HO_{cus} group. The presence of the step edge imposes a slightly different MSI coordination environment on the right side of the model. We designate this site as "Au**(111)−HO_{cus}" to distinguish the two similar MSI sites.

A monolayer of water adsorbed on the support (Scheme 1, bottom) physically blocks adsorbates from interacting with the Au*(111)−HO_{cus} and Au**(111)−HO_{cus} sites. Under these conditions, we describe the catalyst surface on the left side of the model as "Au(111)−H_2O". This indicates proximity between the available 9-coordinate Au(111) site and water adsorbed on the support (not on Au). Similarly, the site defined by water adsorbed on the support and the Au(211) step-edge is described as the "Au(211)−H_2O" site.

Our previous work indicated the fastest H_2 oxidation pathway involves a combination of Au−H deprotonation followed by proton addition to various Au−O species (Au-OOH, Au−H_2O_2, Au−O, and Au−OH).[48] We first address these O_2 activation and subsequent reaction steps, many of which involve proton transfers that might be impacted by an adsorbed water layer. The energetics of these elementary steps at the Au**(111)−HO_{cus} sites (absence of water) and at the Au(211)−H_2O sites (presence of water) are presented in Table 1.

With one exception, the calculated barriers for proton transfer steps at MWI sites are within 0.15 eV of the barriers at MSI sites. The only significant difference is the O_2 activation barrier near HO_{br} sites, which is considerably higher in the presence of water. However, water mediates proton transfer from acidic HO_{br} to basic HO_{cus} sites, and Au−OOH formation using $^{+}H_2O_{cus}$ sites is fast. Thus, the overall proton mediated O_2 activation pathway is largely unchanged by the addition of water. Two proton transfer steps (Au−H deprotonation and Au−H_2O_2 protonation) have modest barriers that affect the coverages of the adsorbed species, but neither step is significantly impacted by the presence of water.

Since the added water layer has a relatively small impact on the overall proton transfer and O_2 activation kinetics, we conclude that the reaction likely proceeds through similar pathways in the presence and absence of exogenous water. Additionally, nearly all proton transfer reactions have barriers lower than 0.2 eV and can be considered quasi-equilibrated under typical reaction conditions. Most importantly, the presence of the water layer has generally small effects on the calculated thermodynamics and kinetics of these steps. While the reaction is conveniently described as limited by hydrogen activation, this is an oversimplification. Our previous kinetics studies indicate that the reaction is H coverage limited rather than strictly limited by H_2 activation.[48] However, H_2 activation has the largest kinetic barrier and is most significantly impacted by the presence of water. The analysis below is not intended to describe the entire reaction network, but focuses on the details of the key first step in the mechanism.

H_2 Activation Thermodynamics. While there may be small differences in the Au coverage of various species, the primary difference between the dry and wet feeds is the water coverage on TiO_2 and therefore surface hydroxyl availability. Hydrogen adsorption reaction energies and associated activation barriers are summarized in Table 2. The left side of Figure 1 shows the final states and their relative energies for H_2 adsorption at the Au*(111)−HO_{cus}, Au(111)−H_2O, and Au(211)−H_2O sites. When the water layer is present, the calculations show the final state has a proton transferred to the support HO_{cus} (Figure 1). This is essentially the same final state as that for H_2 activation directly at the MSI, and it is a consequence of the HO_{cus} being the most basic hydroxyl group in the system.

https://dx.doi.org/10.1021/jacs.9b13729
J. Am. Chem. Soc. 2020, 142, 5760−5772

Table 2. DFT Reaction Energies (ΔE) and Activation Energies (E_a) for H_2 Activation on Various Sites on Au/TiO_2

reaction site	H_2 activation mode	ΔE (eV)	E_a (eV)	ref
Au*(111)−HO_{cus}	heterolytic	−0.03	0.70	ref 48
Au**(111)−HO_{cus}	heterolytic	0.08	0.81	this work
Au(211)−H_2O	heterolytic	0.05	0.99	this work
Au(111)−H_2O	heterolytic	0.29	1.25	this work
Au(111)−Au(111)	homolytic	1.07	1.58	this work
Au(211)−Au(211)	homolytic	0.59	1.16	ref 48

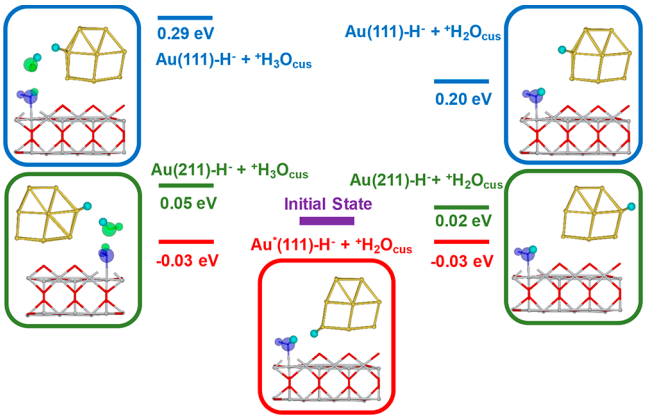

Figure 1. Final states for H_2 adsorption at Au*(111)−OH_{cus} (red), Au(211)−H_2O (left, green), and Au(111)−H_2O (left, blue). The horizontal lines show the calculated reaction energies. The right side of the figure shows the calculated energies for moving the Au−H from the metal−support interface site (Au*(111)−H^-, red) to the Au(211)−H^- (green) and Au(111)−H^- (blue) sites.

The three Au−H adsorption sites are located at chemically distinct Au atoms. To understand water's influence on H_2 adsorption, we first determined the impact of the Au surface atom coordination environment by evaluating how Au−H stability affects H_2 adsorption energy. Using the final state of H_2 adsorption at the Au*(111)−HO_{cus} site (i.e., Au*(111)H^- + $^+H_2O_{cus}$) as the reference state, the hydride was moved to the other two calculated positions and the system energy was calculated. The final states and calculated energies are shown on the right side of Figure 1. The energetic differences associated with moving the Au−H closely mirror the overall energy differences in H_2 adsorption, indicating these differences are almost entirely due to the differences in Au−H stability. We therefore conclude the added water layer, in spite of mediating the proton transfer at the Au(111)−H_2O and Au(211)−H_2O sites, has almost no effect on the H_2 adsorption thermodynamics. The water layer must therefore have large effects on the kinetics and dynamics of H_2 adsorption, which we explore further below.

Experimental Determination of H_2 Oxidation Kinetic Parameters at Constant θ_{H_2O}. Although the measured E_{app} values extracted from constant P_{H_2O} data are determined in a manner consistent with the literature, they miss a key component to this system: under constant water pressure, the support water coverage changes significantly with temperature. Since water blocks the fast H_2 activation sites at the MSI, changing water coverage effectively changes the number of active sites on the catalyst. Over this relatively small temperature range, water coverage (θ_{H_2O}) can change by more than 30%. This significantly impacts the number of available MSI sites. For example, the nominal fraction of exposed hydroxyl groups triples when θ_{H_2O} changes from 0.9 MLE (10% exposed hydroxyls) to 0.7 MLE (30% exposed hydroxyls). We note that this example is illustrative; it is difficult to know the true number of available active hydroxyl groups at the MSI under any given condition.

We therefore carried out experiments at constant water coverage to ensure the accuracy of the experimental measurements. Judicious choice of reaction conditions, careful control of H_2 conversion, and long reaction equilibration times were required to ensure steady-state activity; this allowed us to maintain consistent θ_{H_2O} within reasonable experimental errors. The reaction requirements limited our submonolayer measurements to between 0.8 and 0.9 MLE of water; under these conditions, we believe H_2 activation occurs at the MSI with surface Ti−OH groups.

Table 3. H_2 Oxidation Reaction Orders at $\theta_{H_2O} < 1$ (ref 48) and $\theta_{H_2O} > 1$ (from This Work)

reactant/species	$\theta_{H_2O} < 1$[a]	$\theta_{H_2O} > 1$[b]
O_2	0.20 ± 0.07	0.16 ± 0.05
H_2	0.64 ± 0.05	1.8 ± 0.2
H_2O (wrt pressure)	−0.64 ± 0.02	−1.21 ± 0.07
H_2O (wrt coverage)	−1.41 ± 0.06	−2.8 ± 0.2

[a]Reference 46: P_{H_2}: 23−456 Torr; P_{O_2}: 7.6−76 Torr; P_{H_2O}: 5−18 Torr. T_{rxn} = 60 °C. WHSV: 2.3 × 10^3 L/g_{cat}/h. [b]This work: P_{H_2}: 243−304 Torr; P_{O_2}: 7.6−23 Torr; P_{H_2O}: 9−18 Torr. T_{rxn} = 40 °C. WHSV: 86 L/g_{cat}/h.

Kinetic data collected at low ($\theta_{H_2O} < 1$ MLE) and high ($\theta_{H_2O} > 1$ MLE) θ_{H_2O} are reported in Table 3 and incorporated into observed rate laws (eqs 1 and 2). The O_2 reaction orders are within error of each other, indicating water has no significant effect on O_2 activation. This is consistent with our observations for CO oxidation[8,38,40] and with the elementary step analysis reported in Table 1. The changes in H_2 and H_2O reaction orders were surprisingly large. For $\theta_{H_2O} > 1$ MLE, water inhibition is far more pronounced (i.e., larger negative reaction order) than for MLE water coverages less than unity. The concomitant large increase in the H_2 reaction order indicates the loss in activity is associated with large changes in hydrogen activation kinetics.

$$\text{for } \theta_{H_2O} < 1: \quad \nu_{obs} = k'_{obs}\frac{P_{H_2}^{0.7}P_{O_2}^{0.2}}{\theta_{H_2O}^{1.4}} \tag{1}$$

$$\text{for } \theta_{H_2O} > 1: \quad \nu_{obs} = k'_{obs}\frac{P_{H_2}^{1.8}P_{O_2}^{0.2}}{\theta_{H_2O}^{2.8}} \tag{2}$$

Arrhenius studies were carried out by adjusting the feedwater pressure at each reaction temperature to ensure constant θ_{H_2O} at different reaction temperatures within reasonable experimental errors. Equations 1 and 2 were used to determine k'_{obs} values and normalize the small differences in

https://dx.doi.org/10.1021/jacs.9b13729
J. Am. Chem. Soc. 2020, 142, 5760−5772

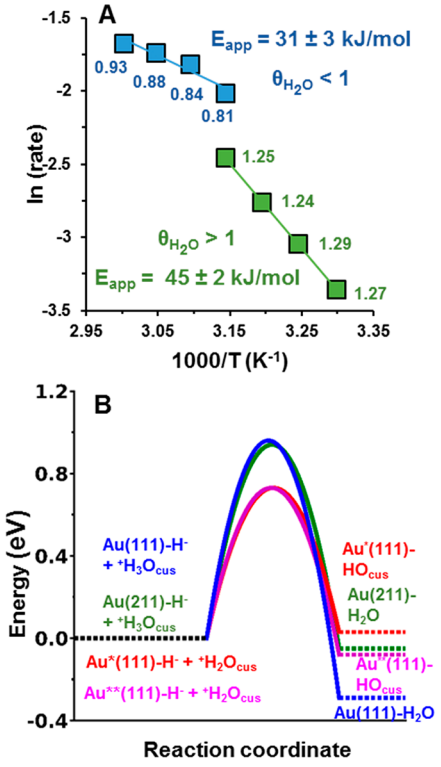

Figure 2. (A) Arrhenius studies at constant water coverage of 0.86 ± 5% MLE (blue) and 1.26 ± 2% MLE (green). Each data point is labeled with the estimated water coverage under the conditions of the experiment. (B) Hydrogen evolution energetics from proton−hydride pairs; reaction energies were referenced to the initial state of the proton−hydride pair.

θ_{H_2O}, which are presented alongside each data point in Figure 2A. Direct plots of the k'_{obs} values are in the Supporting Information.

We also re-examined the 9 Torr constant pressure data, in which θ_{H_2O} was always less than unity, using eq 1 (see the Supporting Information). This yielded an E_{app} value of 26 ± 3 kJ/mol, in good agreement with the constant coverage data (31 ± 3 kJ/mol). We therefore consider the value of 25−30 kJ/mol as our experimental measure of the apparent activation energy for H_2 oxidation at Au-MSI sites. This value is slightly lower than Haruta et al.'s determination for H_2 activation (36 kJ/mol) from H_2−D_2 equilibration kinetics,[59] but the two agree reasonably well. The Arrhenius data for θ_{H_2O} = 1.26 (45 ± 2 kJ/mol) is significantly larger. These E_{app} values (25−30 ± 3 kJ/mol for θ_{H_2O} < 1 and 45 ± 2 kJ/mol for θ_{H_2O} > 1) clearly show the two different kinetic regimes predicted in the density functional theory (DFT) calculations. While the experimental values describe the overall reaction and are therefore imperfect models for H_2 activation, these values represent our best experimental E_{app} measurements for comparison with the computational model.

The principle behind Arrhenius experiments is to measure the rate constant dependence on temperature; however, care must be taken to correlate Arrhenius data with physically meaningful activation barriers. As shown above, dramatically different E_{app} values result from constant water pressure and constant water coverage experiments. Standard Arrhenius studies using constant feed composition involve the intrinsic assumption that coverages remain relatively constant over the temperature range studied.

For many systems, this is a reasonable assumption; however, the concentration of active sites can change when active sites are dynamically created, modified, or destroyed in rapid response to changes in the reaction environment (e.g., temperature or partial pressure). For interfacial reactivity, adsorbates on both the metal and support must be considered. The kinetically important water is weakly adsorbed to the support; as these data show, coverage can change significantly over a relatively small temperature range. Since water masks the support hydroxyl groups that participate in (faster) direct proton transfer from H_2, changes to the water coverage impact the number of available surface hydroxyl groups and thus the reaction kinetics. In such circumstances, coverage must be controlled to keep the catalyst surface in a constant functional state (i.e., maintain a relatively constant number of available support hydroxyl groups) in order to make physically meaningful conclusions from Arrhenius data.

Comparing DFT and Experiments. The absolute values of the experimental E_{app} values, which describe the temperature sensitivity of overall reaction rate constants, cannot be directly compared with DFT barriers calculated for elementary reaction steps. Moreover, the experimental measurements occur over a range of sites, most of which likely have lower coordination numbers than the DFT model and are expected to be more reactive. Further, the experimental values are apparent (not intrinsic) activation energies, and include the complexities of the reaction network. However, the experimental data presented here and published previously[48] collectively suggest the E_{app} values are dominated by the H_2 activation step.

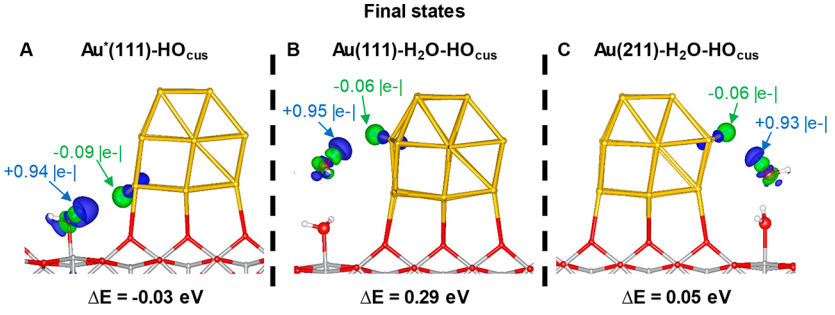

Figure 3. Charge density difference plots for the final states of H_2 activation across (A) the Au*(111)−HO$_{cus}$ site, (B) the Au(111)−H$_2$O site, and (C) the Au(211)−H$_2$O site. Green shading (negative charge) shows electron accumulation, and blue shading (positive charge) shows electron depletion.

https://dx.doi.org/10.1021/jacs.9b13729
J. Am. Chem. Soc. 2020, 142, 5760−5772

Qualitative comparisons with DFT calculations focused on H_2 adsorption are therefore appropriate.

Because each surface Au atom in the DFT model is chemically distinct, we cannot directly compare reactions in the presence and absence of water without accounting for the differences in surface reactivity. To do this, we examined H_2 evolution from the four MSI and MWI active sites, since the principle of microscopic reversibility dictates H_2 evolution and H_2 adsorption must pass through the same transition state. Referencing all the initial states to the same energy also accounts for the energy differences associated with the unique coordination environments of the different Au sites, more clearly identifying the effect of water.

Figure 2B shows this comparison, referencing all of the adsorbed proton−hydride pairs to the same initial energy. Visualized this way, the effect of water on the transition state energy is clear: for this DFT model, the calculated activation barrier is ∼0.2 eV higher in the presence of the water layer. This corresponds to an ∼20 kJ/mol difference between proton transfer directly to a support hydroxyl group and proton transfer mediated by water; the experimental E_{app} values are 15−25 kJ/mol larger when $\theta_{H_2O} > 1$. This constitutes very good qualitative agreement between theory and experiment and imparts greater confidence that conclusions from the DFT calculations have physically meaningful implications for the experimental system.

Charge Distribution After H_2 Adsorption. Additional DFT calculations were directed toward understanding the details of how water impacts the H_2 activation kinetics. Figure 3 shows charge density distributions about the H_2 molecule from final state calculations for H_2 adsorption on three different sites. The final states, which are quite similar in the presence and absence of water, have essentially a full positive charge on the proton, yet only a small partial negative charge on the (formal) hydride.

To identify the distribution of the remaining negative charge, we examined Bader charge differences (final state−initial state) for all atoms in the system (Figure 4). A negative value indicates the corresponding atom/atoms develop additional negative charge, while a positive value indicates positive charge is developed (or negative charge is removed). The positive charge resides almost exclusively on the proton, which is always closely associated with the HO_{cus}. Although H_2 adsorption adds two electrons to the system, there is surprisingly little negative charge on either the Au nanorod or the hydride; rather, the compensating negative charge is highly delocalized, distributed across the hydride, Au, Ti, and remaining support O atoms.

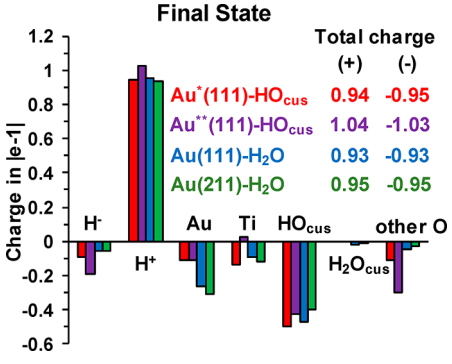

Figure 4. Bader charges of final states (FS) of H_2 activation. Bader charges are referenced with relation to those of the initial state (IS). H^-: hydride; H^+: proton; Au: all gold atoms; Ti: all titanium atoms; HO_{cus}: cus-hydroxyl abstracting the proton; H_2O_{cus}: water molecule abstracting the proton; other O: all other oxygen atoms.

Figure 5 shows the Au(111) side of the model with and without water to further highlight how H_2 adsorption affects the Ti−OH_{cus} bond. Proton transfer to the HO_{cus} induces an ∼0.4 Å increase in the Ti−O bond length; essentially, the combination of the proton transfer and negative charge localization on the HO_{cus} partially pulls the OH group out of the plane of the TiO_2 surface. This change in the final state geometry is consistent throughout the calculations regardless of the presence or absence of the water layer, and did not depend significantly on the Au atom(s) involved in stabilizing the hydride (see the Supporting Information for further details). This is a substantial surface restructuring and is supported by experimental FTIR measurements.

Infrared Spectroscopy during H_2 Adsorption. We previously showed H_2 adsorption on Au was observable in FTIR spectra by exchanging support hydroxyl protons with deuterons.[48] Experimental evidence for surface structural changes during CO adsorption on Au/TiO_2 has also been reported.[60] In that study, CO adsorption correlated with an overall loss of light transmission through the sample, which was observed as a "broad band IR" (BB-IR) absorption and quantitatively correlated with the IR absorption band associated with CO adsorbed on Au.[61] The effect was concluded to arise from decreased light transmittance associated with surface roughening of the titania, which was hypothesized to arise from electron transfer to the support from Au upon H_2 adsorption.[60]

Experimental evidence for the structural changes induced by H_2 adsorption can be found in infrared spectra collected after deuterated Au/TiO_2 is exposed to H_2 (Figure 6). These spectra contain various features including water bending vibrations (1500−1800 cm^{-1}), hydroxyl stretching vibrations (2800−3700 cm^{-1}) and the broad band baseline shift. We monitored the BB-IR signal by determining the area under the IR spectral curve from 1800 to 2100 cm^{-1}, and 3800−3950 cm^{-1}, as was previously reported for static CO adsorption measurements.[60] Measuring the BB-IR signal over time at various temperatures (50−70 °C) provided an independent measure of the H_2 activation kinetic barrier.

Panayotov and Yates employed a similar approach using IR absorbance data to determine the H_2 activation barrier on Au/TiO_2 in their system.[62] We note that this description of surface roughening, and a general method for evaluating H_2 adsorption was described by Pollock, Peterson, and Pursell using static H_2 adsorption experiments.[61] Yates and Morris reported similar findings, describing their IR spectra in terms of H atom spillover.[62−64] A proton and electron transferred to the support can be considered as equivalent to H atom spillover,[65] so Yates and Morris' interpretation is consistent with our findings. Similar changes to IR spectra have also been reported during low temperature (90 K) photoexcitation of titania, and suggested to be caused by the injection of electrons into the titania conduction band.[66] Our observations are also broadly consistent with this interpretation.

The extracted kinetic data are shown in panels B and C of Figure 6; Arrhenius plots are shown in panel D. The activation barrier measured with the BB-IR signal was 25 ± 2 kJ/mol for the 1800−2100 cm^{-1} region and 20 ± 1 kJ/mol for the 3800−

https://dx.doi.org/10.1021/jacs.9b13729
J. Am. Chem. Soc. 2020, 142, 5760−5772

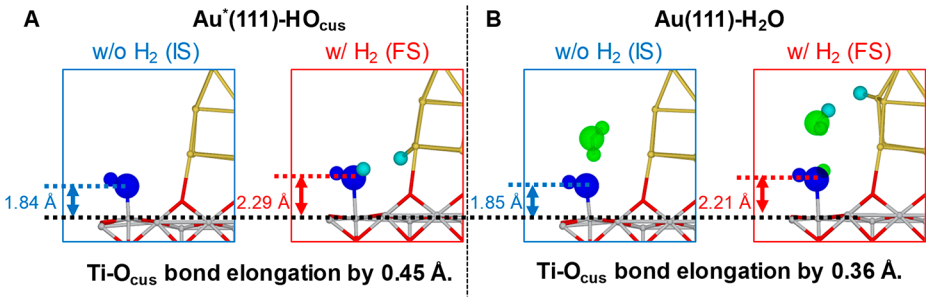

Figure 5. Variation of the Ti−O_{cus} bond length upon H_2 adsorption across the Au(111) facet at (A) the MSI site and (B) the MWI site.

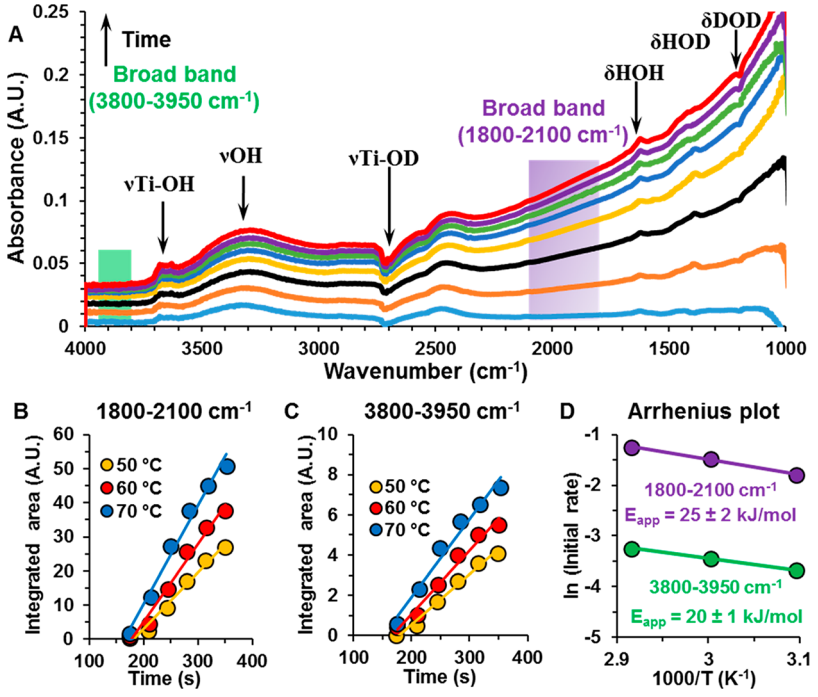

Figure 6. (A) FTIR spectra of H_2 adsorption on a D_2O-exchanged Au/TiO_2 catalyst. Reaction conditions: T: 50 °C, WHSV = 40 L/g_{cat}/h. Temperature dependence of the integrated area under the spectral regions: (B) 1800−2100 cm^{-1} and (C) 3800−3950 cm^{-1}. (D) Arrhenius fit of initial rates of different spectral regions during H_2 adsorption on Au/TiO_2.

3950 cm^{-1} spectral region. These values, which we interpret as estimates of E_{app} for H_2 adsorption when $\theta_{H_2O} < 1$ MLE, agree well with the E_{app} value determined in the reaction kinetics (i.e., packed bed reactor studies). Considering that no O_2 or additional H_2O/D_2O was present in the feed during the IR experiments, the IR data support the conclusion that the E_{app} value measured during H_2 oxidation kinetics is dominated by H_2 adsorption. Thus, all of the E_{app} measurements are internally consistent. They therefore provide a strong experimental foundation for focusing the DFT calculations on the dominant H_2 adsorption reaction.

Electronic Changes Associated with H_2 Adsorption. The observation and characterization of this large structural change prompted us to more carefully examine the structural and electronic changes that result from H_2 adsorption. While the Au−H species is a formal hydride for electron counting purposes, there is relatively little charge on the H atom in the final state. This indicates the Au−H bond is largely covalent with significant electron donation into the Au nanorod. This is not surprising given that Au is slightly more electronegative than hydrogen. While many refer to this species as a "hydrogen atom" we maintain the description of a formal hydride in order to scrupulously maintain electron counting and distinguish between the proton and hydride.

We also compared the Bader charges on the water-free structures to the calculated reaction energies. The small variance in the negative charges were normalized to a total charge of −1; this normalization was ∼5% of the total charge (details in the Supporting Information). In broad terms, the distribution of negative charge is similar in all these structures: about 1/4 of an electron remains distributed between the hydride and the Au nanorod, about 1/2 of an electron is localized on the HO_{cus}, and about 1/4 of an electron is distributed across the rest of the support (Ti and O atoms, see SI Table S1 for details). The only broad correlation between the final state energies and the distributed charges was in the relative amounts of charge on the hydride and the Au nanorod. This is shown in Figure 7, which includes a plot showing the correlation between final state energy and the fraction of negative charge on the Au nanorod.

Based on Figure 7, it is unclear if this correlation is due to the destabilization of Au as excess negative charge builds on the nanorod, or if the hydride works to withdraw electron density from the system. Given the similar electronegativities

https://dx.doi.org/10.1021/jacs.9b13729
J. Am. Chem. Soc. 2020, 142, 5760−5772

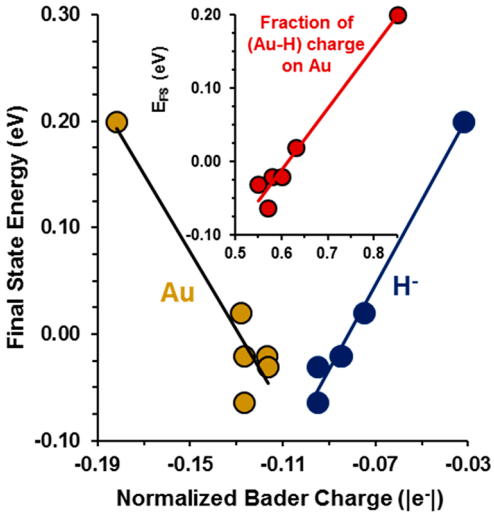

Figure 7. Hydrogen adsorption final state energies plotted against the Bader charge on the formal hydride and the Au nanorod. The inset shows the energy as a function of the fraction of the total Au + H^- charge on the Au nanorod.

of Au and H, it may be that the system is simply most stable when the negative charge is spread more or less evenly over these two parts of the system. This is tied to the reactivity of the specific surface site: less reactive surface sites (i.e., 9-coordinate Au(111) sites) are already electronically saturated. We note that this is also consistent with the broader chemistry of Au. With a full d-band and half full s-band, Au is electronically stable. This drives the propensity for heterolytic H−H activation, which avoids the formal oxidation associated with dissociative chemisorption. Similarly, excess electron density overpopulates the s-band, so the system transfers the electron density to the support. In this case, it largely localizes on the most electronegative atom in the system (HO_{cus}) where it stabilizes the generated proton. The reaction might therefore be considered as going through a proton coupled electron transfer-type mechanism.

As discussed above, the water layer causes negligible changes in the overall reaction energy (<0.1 eV, Figure 1, Table S1). However, water perturbs the final state charge distribution, shifting ~0.1−0.2 electrons onto the Au at the expense of the support. The charge on the proton, which resides on the HO_{cus}, remains very close to the +1 electron, so it is not immediately obvious why water stabilizes greater charge on the nanorod. One possibility is that the water layer, which extends along the length of the nanorod, provides a weak solvation effect that helps to stabilize greater charge density on the Au surface.

Semiquantitative Structural and Electronic Analysis of H_2 Activation. Calculated transition states (Figure 8) show the influence of water on H_2 activation kinetics/dynamics; structural data can be found in Figure 9A and in the

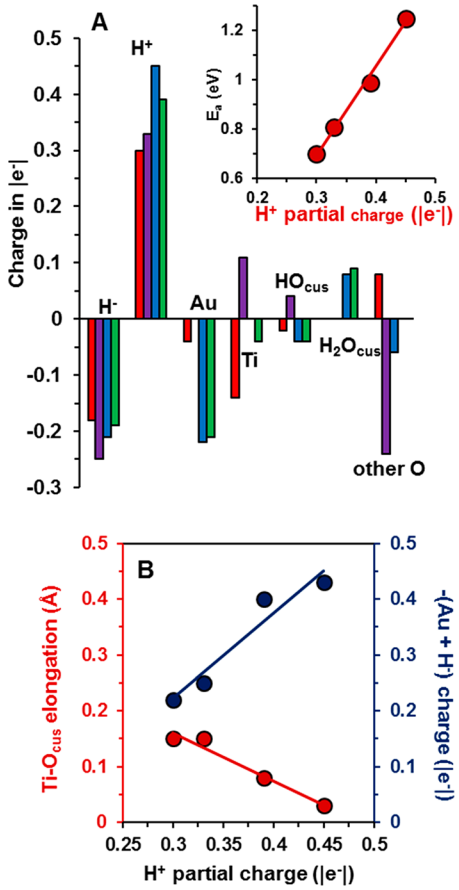

Figure 9. Transition state charge distribution and structural changes. (A) H_2 activation transition state (TS) Bader charges. Bader charges are referenced to the initial state (IS). H^-: hydride; H^+: proton; Au: all gold atoms; Ti: all titanium atoms; HO_{cus}: cus-hydroxyl abstracting the proton; H_2O_{cus}: water molecule abstracting the proton; other O: all other oxygen atoms. The inset shows the calculated H_2 activation energies plotted against the partial charge of the developing proton. (B) Ti−O_{cus} bond length and the sum of gold and hydride charge in the H_2 activation transition state plotted against the proton partial charge for various sites at the MSI and MWI of Au/TiO_2.

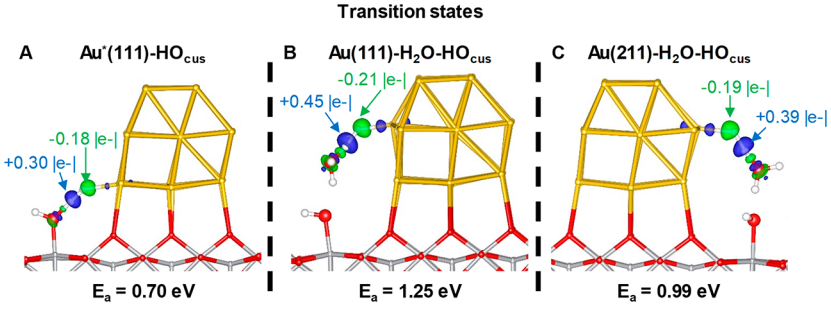

Figure 8. Charge density difference plots of transition states for H_2 activation across (A) Au*(111)−HO_{cus}, (B) Au(111)−H_2O, and (C) Au(211)−H_2O. Green shading (negative charge) shows electron accumulation, and blue shading (positive charge) shows electron depletion.

https://dx.doi.org/10.1021/jacs.9b13729
J. Am. Chem. Soc. 2020, 142, 5760−5772

Supporting Information. The calculated activation barrier correlates closely with the degree of charge buildup on the developing proton (Figure 9A). The total charge on the Au and hydride also tracks with this value, as does the H−H bond distance (see the Supporting Information). Thus, the higher barrier is associated with greater charge separation and a later transition state. Notably, the charge on the hydride is relatively similar in all four structures; most of the additional charge associated with the later transition state is distributed across the Au nanorod. Additionally, there is surprisingly little charge distributed to the HO_{cus} or the support in any of the transition states.

The underlying phenomenon we would like to understand is why/how the water layer shifts the reaction to a later, higher energy transition state. A clue to this question lies in the structural changes associated with the HO_{cus} group. Figure 9B shows the negative charge buildup on the hydride and Au nanorod plotted against the charge on the developing proton. As suggested above, these correlate with greater negative charge developing to compensate the positive charge. However, the Ti−O bond shows exactly the opposite trend. Based on the final state geometry, the Ti−O bond eventually undergoes an ∼0.4 Å elongation; however, in the later transition states, the Ti−O bond is slightly shorter than in the initial state. As Figure 9B shows, this strong correlation suggests an important difference in the presence of water.

It appears that H_2 activation proceeds through a proton-coupled electron transfer (PCET)-like mechanism. The HO_{cus} carries relatively little charge in any of the transition states, suggesting that the positive charge is required to facilitate electron transfer to the support. Even though proton transfers are relatively fast, the water layer imposes a transport barrier to moving the positive charge, slowing that process. This, in turn, forces greater negative charge buildup on the Au nanorod, which the final state calculations show is a net destabilizing influence on the system. Thus, water appears to slow H_2 activation by slowing the proton transfer to the support OH groups, which is a necessary precondition for fast electron transfer from Au to the support.

We initially concluded that water poisoning of H_2 oxidation resulted from simple blocking of the fastest reaction sites at the MSI. While this is certainly true, the details of this poisoning are more complicated and illuminating. In particular, the poisoning appears to occur by slowing the dynamics of charge transfer between the Au and the support; this is a far more dynamic representation of the active site than can be understood with a simple site blocking model. Further, it indicates that both proton and electron transfer play important roles in H_2 activation; this likely has implications for similar systems.

Hydrogen Spillover and Reducible Supports. Hydrogen activation over Au can considered in the context of two limiting descriptions of this chemistry: support reduction and hydrogen spillover. The process involves the transfer of both a proton and an electron to the support. Since a proton and electron can be reasonably considered as equivalent to a hydrogen atom,[65] it can also be described as "hydrogen spillover". Similarly, H_2 activation over Au involves the transfer of charge to the support and partial localization of the charge onto a surface hydroxyl. While this might more aptly be described as a redistribution and localization of charge within the system, it is still consistent with the concept of support reduction.

However, the transfer of negative charge to the support described by the DFT model presents a remarkably different picture of "support reduction" than is commonly considered. Typically, a "reducible support" such as TiO_2 implies that metal sites can be reduced and/or oxygen vacancies produced, as in the classic Mars van Krevelen mechanism. Behm's group in particular has provided compelling evidence for the role of O vacancies in CO and H_2 oxidation over Au/TiO_2 above ∼100 °C.[9,67−69] Under the conditions of our experiments, where monolayer equivalents of water are present at relatively low temperatures, O vacancies cannot be reasonably invoked as participants in the reaction mechanism. Instead, support reducibility in this case is governed by the ability/necessity of stabilizing protons and electrons on the support, not by the propensity to form O vacancies.

It is also worth noting that, in the context of the formalisms associated with oxidation states and electron counting, there is no "formal" reduction of the support during hydrogen activation. Both formal oxidation states and organometallic electron counting schemes are valuable for understanding these systems, but both are ultimately limiting descriptions of the chemistry and should be considered in appropriate context. In this case, H_2 activation is properly considered as heterolytic, generating a proton on the support and a formal hydride on the Au. This process is driven by the well-known disinclination of Au to undergo oxidation. However, this description, while valuable and necessary to maintain charge neutrality in describing the process, is ultimately limiting. The reality, at least as suggested by the DFT calculations, is that the negative charge of the hydride is distributed throughout the system through the Au. In this sense, the Au functions as a nanowire to distribute one of the electrons in the H−H bond throughout the system.

The oxidation states typically used to describe the support (e.g., Ti(IV) and O^{2-}) are similarly limiting descriptions. While these descriptions are necessary to maintain charge neutrality and provide categories for broad descriptive chemistries, the reality is more complex with electrons shared between the formal oxide and formal Ti(IV). Numerous other models, including of course band theory, provide other more detailed but similarly limiting descriptions of these interactions. Thus, the support does not undergo a "formal" reduction during H_2 activation in the sense of generating a Ti(III) site or producing an O vacancy. Rather, the charge in the system is partially redistributed and localized on a surface hydroxyl group where it can stabilize (or is stabilized by) the proton.

This description or interpretation has the appeal of transferring/localizing charge onto the most electronegative atom(s) in the system. Further, because it does not require formal reduction of a support cation, it is likely to be a more general description of this chemistry. This is important for supported Au catalysts, where reducible and nonreducible supports can show similar chemistries. This is particularly true for CO and H_2 oxidation, which show nearly identical kinetics over Au/TiO_2 and Au/Al_2O_3, at least under conditions where water coverage is controlled.[38,48] Thus, beyond expanding our understanding of how "support reducibility" can be considered, this study provides a clear example of how reducible and nonreducible supports can influence reaction rates through subtle changes in electronics, without necessitating the invocation of larger formal electron transfers.[70]

https://dx.doi.org/10.1021/jacs.9b13729
J. Am. Chem. Soc. 2020, 142, 5760−5772

Finally, we note the complex interplay between metal, support, protons, and electrons evidenced in this chemistry provide new ways to think about reactions at the metal−support interface. As noted by a reviewer of this paper, this study shows how adsorbates on the metal and at the metal−support interface can modify the broader electronic structure of the catalyst. Adsorbate-modified catalysts may similarly have lower energy reaction pathways available that have not been previously considered. This may be particularly useful for similar reactions over d^{10} metals where the metal−support interface is known to be important, such as alkyne partial hydrogenation over Au[71−77] or Ag,[78] CO_2 hydrogenation over Cu based catalysts,[2−5] or methanol synthesis catalysts.[6]

CONCLUSION

This study highlights the complex and multiple ways that adsorbed water can impact catalysis over supported nanoparticles. The strong product poisoning imposes the experimentally challenging requirement that kinetic parameters be determined at constant water coverage in order to maintain a consistent number of metal−support interface sites. The mechanism of water poisoning and the insight it provides into the reactivity of Au catalysts are particularly noteworthy. Rate limiting hydrogen activation appears to go through a PCET-like mechanism, whereby a proton from H_2 is transferred to a support hydroxyl group. The associated negative charge is distributed across the formal hydride, the Au, and the support, with the largest concentration of charge on the hydroxyl group to which the proton was transferred. Water slows this process by providing a transport barrier to moving the proton to the support hydroxyl group. This pushes the reaction to a later transition state, forcing greater (and unfavorable) negative charge buildup on the Au, thereby increasing the transition state energy by ∼0.2 eV. A similar change in apparent activation energy was determined experimentally through reaction kinetics and *in situ* infrared spectroscopic studies.

ASSOCIATED CONTENT

Supporting Information

The Supporting Information is available free of charge at https://pubs.acs.org/doi/10.1021/jacs.9b13729.

Methods and materials; development details of DFT model water layer; effect of hydride position on H_2 dissociation energetics; DFT examination of H_2 activation across the MWI sites; DFT charge analysis; DFT bond length analysis; additional kinetics data (PDF)

AUTHOR INFORMATION

Corresponding Author

Bert D. Chandler − *Department of Chemistry, Trinity University, San Antonio, Texas 78212-7200, United States;* orcid.org/0000-0002-8621-0361; Email: Bert.chandler@trinity.edu

Authors

K. B. Sravan Kumar − *Department of Chemistry, Trinity University, San Antonio, Texas 78212-7200, United States; Department of Chemical and Biomolecular Engineering, University of Houston, Houston, Texas 77204-4004, United States*

Todd N. Whittaker − *Department of Chemistry, Trinity University, San Antonio, Texas 78212-7200, United States*

Christine Peterson − *Department of Chemistry, Trinity University, San Antonio, Texas 78212-7200, United States*

Lars C. Grabow − *Department of Chemical and Biomolecular Engineering, University of Houston, Houston, Texas 77204-4004, United States;* orcid.org/0000-0002-7766-8856

Complete contact information is available at: https://pubs.acs.org/10.1021/jacs.9b13729

Author Contributions

§K.B.S.K. and T.N.W. contributed equally to the work.

Notes

The authors declare no competing financial interest.

ACKNOWLEDGMENTS

The authors gratefully acknowledge the National Science Foundation (Grants CHE-1465148, CHE-1465184, and CBET-1803769) and the Research Corporation for Science Advancement for supporting this work. The authors thank Prof. Siris Laursen and Evan Williams for helpful discussions. B.D.C. thanks Profs. Jeff Bode and Christophe Copéret as well as the Laboratorium für Organische Chemie and the Laboratorium für Anorganische Chemie at ETH Zürich for support during his academic leave. Computational resources were provided by the uHPC cluster managed by the University of Houston and acquired through NSF-MRI award number 1531814. This work used the Extreme Science and Engineering Discovery Environment (XSEDE), which was supported by NSF grant number ACI-1053575.[79] We also acknowledge the use of computational resources provided by the National Energy Research Scientific Computing Center, a DOE Office of Science User Facility supported by the Office of Science of the US Department of Energy under contract number DE-AC02- 05CH11231. The authors acknowledge the use of the Maxwell/Opuntia/Sabine Cluster and the advanced support from the Core Facility for Advanced Computing and Data Science at the University of Houston to carry out parts of the research presented here.

REFERENCES

(1) Ponec, V.; Bond, G. C. *Catalysis by Metals and Alloys*; Elsevier: Amsterdam, 1995; Vol. 95.

(2) Kattel, S.; Yan, B.; Yang, Y.; Chen, J. G.; Liu, P. Optimizing Binding Energies of Key Intermediates for CO2 Hydrogenation to Methanol over Oxide-Supported Copper. *J. Am. Chem. Soc.* **2016**, *138* (38), 12440−12450.

(3) Kattel, S.; Ramirez, P. J.; Chen, J. G.; Rodriguez, J. A.; Liu, P. Active sites for CO2 hydrogenation to methanol on Cu/ZnO catalysts. *Science (Washington, DC, U. S.)* **2017**, *355* (6331), 1296−1299.

(4) Larmier, K.; Liao, W.-C.; Tada, S.; Lam, E.; Verel, R.; Bansode, A.; Urakawa, A.; Comas-Vives, A.; Coperet, C. CO2-to-Methanol Hydrogenation on Zirconia-Supported Copper Nanoparticles: Reaction Intermediates and the Role of the Metal-Support Interface. *Angew. Chem., Int. Ed.* **2017**, *56* (9), 2318−2323.

(5) Lam, E.; Larmier, K.; Noh, G.; Wolf, P.; Comas-Vives, A.; Coperet, C.; Corral-Perez, J. J.; Urakawa, A. CO2 Hydrogenation on Cu/Al2 O3: Role of the Metal/Support Interface in Driving Activity and Selectivity of a Bifunctional Catalyst. *Angew. Chem., Int. Ed.* **2019**, *58* (39), 13989−13996.

(6) Behrens, M.; Studt, F.; Kasatkin, I.; Kuehl, S.; Haevecker, M.; Abild-Pedersen, F.; Zander, S.; Girgsdies, F.; Kurr, P.; Kniep, B.-L.; Tovar, M.; Fischer, R. W.; Norskov, J. K.; Schloegl, R. The Active Site

of Methanol Synthesis over Cu/ZnO/Al2O3 Industrial Catalysts. *Science (Washington, DC, U. S.)* **2012**, *336* (6083), 893−897.
(7) Robinson, A. M.; Hensley, J. E.; Medlin, J. W. Bifunctional Catalysts for Upgrading of Biomass-Derived Oxygenates: A Review. *ACS Catal.* **2016**, *6* (8), 5026−5043.
(8) Saavedra, J.; Doan, H. A.; Pursell, C. J.; Grabow, L. C.; Chandler, B. D. The critical role of water at the gold-titania interface in catalytic CO oxidation. *Science* **2014**, *345* (6204), 1599−1602.
(9) Wang, Y.; Widmann, D.; Heenemann, M.; Diemant, T.; Biskupek, J.; Schloegl, R.; Behm, R. J. The role of electronic metal-support interactions and its temperature dependence: CO adsorption and CO oxidation on Au/TiO2 catalysts in the presence of TiO2 bulk defects. *J. Catal.* **2017**, *354*, 46−60.
(10) Green, I. X.; Tang, W.; Neurock, M.; Yates, J. T., Jr. Spectroscopic Observation of Dual Catalytic Sites During Oxidation of CO on a Au/TiO2 Catalyst. *Science* **2011**, *333*, 736−739.
(11) Carrasquillo-Flores, R.; Ro, I.; Kumbhalkar, M. D.; Burt, S.; Carrero, C. A.; Alba-Rubio, A. C.; Miller, J. T.; Hermans, I.; Huber, G. W.; Dumesic, J. A. Reverse Water-Gas Shift on Interfacial Sites Formed by Deposition of Oxidized Molybdenum Moieties onto Gold Nanoparticles. *J. Am. Chem. Soc.* **2015**, *137* (32), 10317−10325.
(12) Zhao, Z.-J.; Li, Z.; Cui, Y.; Zhu, H.; Schneider, W. F.; Delgass, W. N.; Ribeiro, F.; Greeley, J. Importance of metal-oxide interfaces in heterogeneous catalysis: A combined DFT, microkinetic, and experimental study of water-gas shift on Au/MgO. *J. Catal.* **2017**, *345*, 157−169.
(13) Wang, L.; Zhang, J.; Wang, H.; Shao, Y.; Liu, X.; Wang, Y.-Q.; Lewis, J. P.; Xiao, F.-S. Activity and Selectivity in Nitroarene Hydrogenation over Au Nanoparticles on the Edge/Corner of Anatase. *ACS Catal.* **2016**, *6* (7), 4110−4116.
(14) Corma, A.; Serna, P. Chemoselective Hydrogenation of Nitro Compounds with Supported Gold Catalysts. *Science* **2006**, *313* (5785), 332−334.
(15) Zhu, Y. P.; Guo, C.; Zheng, Y.; Qiao, S.-Z. Surface and Interface Engineering of Noble-Metal-Free Electrocatalysts for Efficient Energy Conversion Processes. *Acc. Chem. Res.* **2017**, *50* (4), 915−923.
(16) Song, F.; Li, W.; Yang, J.; Han, G.; Yan, T.; Liu, X.; Rao, Y.; Liao, P.; Cao, Z.; Sun, Y. Interfacial Sites between Cobalt Nitride and Cobalt Act as Bifunctional Catalysts for Hydrogen Electrochemistry. *ACS Energy Lett.* **2019**, *4* (7), 1594−1601.
(17) Ro, I.; Resasco, J.; Christopher, P. Approaches for Understanding and Controlling Interfacial Effects in Oxide-Supported Metal Catalysts. *ACS Catal.* **2018**, *8* (8), 7368−7387.
(18) Mehta, P.; Greeley, J.; Delgass, W. N.; Schneider, W. F. Adsorption Energy Correlations at the Metal-Support Boundary. *ACS Catal.* **2017**, *7* (7), 4707−4715.
(19) Schauermann, S.; Nilius, N.; Shaikhutdinov, S.; Freund, H.-J. Nanoparticles for Heterogeneous Catalysis: New Mechanistic Insights. *Acc. Chem. Res.* **2013**, *46* (8), 1673−1681.
(20) Campbell, C. T. Catalyst-support interactions: Electronic perturbations. *Nat. Chem.* **2012**, *4* (8), 597−598.
(21) Liu, Z.; Grinter, D. C.; Lustemberg, P. G.; Nguyen-Phan, T.-D.; Zhou, Y.; Luo, S.; Waluyo, I.; Crumlin, E. J.; Stacchiola, D. J.; Zhou, J.; Carrasco, J.; Busnengo, H. F.; Ganduglia-Pirovano, M. V.; Senanayake, S. D.; Rodriguez, J. A. Dry Reforming of Methane on a Highly-Active Ni-CeO2 Catalyst: Effects of Metal-Support Interactions on C-H Bond Breaking. *Angew. Chem., Int. Ed.* **2016**, *55* (26), 7455−7459.
(22) Bruix, A.; Rodriguez, J. A.; Ramirez, P. J.; Senanayake, S. D.; Evans, J.; Park, J. B.; Stacchiola, D.; Liu, P.; Hrbek, J.; Illas, F. A New Type of Strong Metal-Support Interaction and the Production of H2 through the Transformation of Water on Pt/CeO2(111) and Pt/CeOx/TiO2(110) Catalysts. *J. Am. Chem. Soc.* **2012**, *134* (21), 8968−8974.
(23) Lykhach, Y.; Kozlov, S. M.; Skala, T.; Tovt, A.; Stetsovych, V.; Tsud, N.; Dvorak, F.; Johanek, V.; Neitzel, A.; Myslivecek, J.; Fabris, S.; Matolin, V.; Neyman, K. M.; Libuda, J. Counting electrons on supported nanoparticles. *Nat. Mater.* **2016**, *15* (3), 284−288.
(24) Divins, N. J.; Angurell, I.; Escudero, C.; Perez-Dieste, V.; Llorca, J. Influence of the support on surface rearrangements of bimetallic nanoparticles in real catalysts. *Science (Washington, DC, U. S.)* **2014**, *346* (6209), 620−623.
(25) Huang, L.; Han, B.; Xi, Y.; Forrey, R. C.; Cheng, H. Influence of Charge on the Reactivity of Supported Heterogeneous Transition Metal Catalysts. *ACS Catal.* **2015**, *5* (8), 4592−4597.
(26) Pacchioni, G. Electronic interactions and charge transfers of metal atoms and clusters on oxide surfaces. *Phys. Chem. Chem. Phys.* **2013**, *15* (6), 1737−1757.
(27) Hartadi, Y.; Behm, R.; Widmann, D. Competition of CO and H2 for Active Oxygen Species during the Preferential CO Oxidation (PROX) on Au/TiO2 Catalysts. *Catalysts* **2016**, *6* (2), 21.
(28) Karim, W.; Spreafico, C.; Kleibert, A.; Gobrecht, J.; VandeVondele, J.; Ekinci, Y.; van Bokhoven, J. A. Catalyst support effects on hydrogen spillover. *Nature* **2017**, *541*, 68.
(29) Briggs, N. M.; Barrett, L.; Wegener, E. C.; Herrera, L. V.; Gomez, L. A.; Miller, J. T.; Crossley, S. P. Identification of active sites on supported metal catalysts with carbon nanotube hydrogen highways. *Nat. Commun.* **2018**, *9* (1), 1−7.
(30) Liu, J.; Hibbitts, D.; Iglesia, E. Dense CO Adlayers as Enablers of CO Hydrogenation Turnovers on Ru Surfaces. *J. Am. Chem. Soc.* **2017**, *139* (34), 11789−11802.
(31) Hibbitts, D.; Dybeck, E.; Lawlor, T.; Neurock, M.; Iglesia, E. Preferential activation of CO near hydrocarbon chains during Fischer−Tropsch synthesis on Ru. *J. Catal.* **2016**, *337*, 91−101.
(32) Wang, Y.-G.; Cantu, D. C.; Lee, M.-S.; Li, J.; Glezakou, V.-A.; Rousseau, R. CO Oxidation on Au/TiO2: Condition-Dependent Active Sites and Mechanistic Pathways. *J. Am. Chem. Soc.* **2016**, *138* (33), 10467−10476.
(33) Polierer, S.; Jelic, J.; Pitter, S.; Studt, F. On the Reactivity of the Cu/ZrO2 System for the Hydrogenation of CO2 to Methanol: A Density Functional Theory Study. *J. Phys. Chem. C* **2019**, *123* (44), 26904−26911.
(34) Lakshmanan, P.; Park, J.; Park, E. Recent Advances in Preferential Oxidation of CO in H2 Over Gold Catalysts. *Catal. Surv. Asia* **2014**, *18* (2−3), 75−88.
(35) Ivanova, S.; Pitchon, V.; Petit, C.; Caps, V. Support Effects in the Gold-Catalyzed Preferential Oxidation of CO. *ChemCatChem* **2010**, *2*, 556−563.
(36) Nilekar, A. U.; Alayoglu, S.; Eichhorn, B.; Mavrikakis, M. Preferential CO Oxidation in Hydrogen: Reactivity of Core-Shell Nanoparticles. *J. Am. Chem. Soc.* **2010**, *132* (21), 7418−7428.
(37) Rossignol, C.; Arrii, S.; Morfin, F.; Piccolo, L.; Caps, V.; Rousset, J.-L. Selective oxidation of CO over model gold-based catalysts in the presence of H2. *J. Catal.* **2005**, *230* (2), 476−483.
(38) Saavedra, J.; Pursell, C. J.; Chandler, B. D. CO Oxidation Kinetics over Au/TiO2 and Au/Al2O3 Catalysts: Evidence for a Common Water-Assisted Mechanism. *J. Am. Chem. Soc.* **2018**, *140* (10), 3712−3723.
(39) Saavedra, J.; Powell, C.; Panthi, B.; Pursell, C. J.; Chandler, B. D. CO oxidation over Au/TiO2 catalyst: Pretreatment effects, catalyst deactivation, and carbonates production. *J. Catal.* **2013**, *307*, 37−47.
(40) Saavedra, J.; Whittaker, T.; Chen, Z.; Pursell, C. J.; Rioux, R. M.; Chandler, B. D. Controlling activity and selectivity using water in the Au-catalysed preferential oxidation of CO in H2. *Nat. Chem.* **2016**, *8* (6), 584−589.
(41) Tran, H.-V.; Doan, H. A.; Chandler, B. D.; Grabow, L. C. Water-assisted oxygen activation during selective oxidation reactions. *Curr. Opin. Chem. Eng.* **2016**, *13*, 100−108.
(42) Paulus, U. A.; Wang, Y.; Kim, S. H.; Geng, P.; Wintterlin, J.; Jacobi, K.; Ertl, G. Inhibition of CO oxidation on RuO2(110) by adsorbed H2O molecules. *J. Chem. Phys.* **2004**, *121* (22), 11301−11308.
(43) Daté, M.; Haruta, M. Moisture Effect on CO Oxidation over Au/TiO2 Catalyst. *J. Catal.* **2001**, *201* (2), 221−224.
(44) Ojeda, M.; Zhan, B.-Z.; Iglesia, E. Mechanistic interpretation of CO oxidation turnover rates on supported Au clusters. *J. Catal.* **2012**, *285* (1), 92−102.

https://dx.doi.org/10.1021/jacs.9b13729
J. Am. Chem. Soc. 2020, 142, 5760−5772

(45) Calla, J. T.; Davis, R. J. Influence of Dihydrogen and Water Vapor on the Kinetics of CO Oxidation over Au/Al2O3. *Ind. Eng. Chem. Res.* **2005**, *44* (14), 5403−5410.
(46) Widmann, D.; Behm, R. J. Activation of Molecular Oxygen and the Nature of the Active Oxygen Species for CO Oxidation on Oxide Supported Au Catalysts. *Acc. Chem. Res.* **2014**, *47* (3), 740−749.
(47) Yan, T.; Gong, J.; Flaherty, D. W.; Mullins, C. B. The Effect of Adsorbed Water in CO Oxidation on Au/TiO2(110). *J. Phys. Chem. C* **2011**, *115* (5), 2057−2065.
(48) Whittaker, T.; Kumar, K. B. S.; Peterson, C.; Pollock, M. N.; Grabow, L. C.; Chandler, B. D. H2 Oxidation over Supported Au Nanoparticle Catalysts: Evidence for Heterolytic H2 Activation at the Metal-Support Interface. *J. Am. Chem. Soc.* **2018**, *140* (48), 16469−16487.
(49) Werner, K.; Weng, X.; Calaza, F.; Sterrer, M.; Kropp, T.; Paier, J.; Sauer, J.; Wilde, M.; Fukutani, K.; Shaikhutdinov, S.; Freund, H.-J. Toward an Understanding of Selective Alkyne Hydrogenation on Ceria: On the Impact of O Vacancies on H2 Interaction with CeO2(111). *J. Am. Chem. Soc.* **2017**, *139* (48), 17608−17616.
(50) Dahal, A.; Mu, R.; Lyubinetsky, I.; Dohnálek, Z. Hydrogen adsorption and reaction on RuO2(110). *Surf. Sci.* **2018**, *677*, 264−270.
(51) Hu, G.; Wu, Z.; Jiang, D.-e. First Principles Insight into H2 Activation and Hydride Species on TiO2 Surfaces. *J. Phys. Chem. C* **2018**, *122* (35), 20323−20328.
(52) Huang, Z.-Q.; Liu, L.-P.; Qi, S.; Zhang, S.; Qu, Y.; Chang, C.-R. Understanding All-Solid Frustrated-Lewis-Pair Sites on CeO2 from Theoretical Perspectives. *ACS Catal.* **2018**, *8* (1), 546−554.
(53) Liu, W.; Chen, Y.; Qi, H.; Zhang, L.; Yan, W.; Liu, X.; Yang, X.; Miao, S.; Wang, W.; Liu, C.; Wang, A.; Li, J.; Zhang, T. A Durable Nickel Single-Atom Catalyst for Hydrogenation Reactions and Cellulose Valorization under Harsh Conditions. *Angew. Chem.* **2018**, *130* (24), 7189−7193.
(54) Riley, C.; Zhou, S.; Kunwar, D.; De La Riva, A.; Peterson, E.; Payne, R.; Gao, L.; Lin, S.; Guo, H.; Datye, A. Design of Effective Catalysts for Selective Alkyne Hydrogenation by Doping of Ceria with a Single-Atom Promotor. *J. Am. Chem. Soc.* **2018**, *140* (40), 12964−12973.
(55) Shen, Y.; Yin, K.; An, C.; Xiao, Z. Design of a difunctional Zn-Ti LDHs supported PdAu catalyst for selective hydrogenation of phenylacetylene. *Appl. Surf. Sci.* **2018**, *456*, 1−6.
(56) Phadke, N. M.; Mansoor, E.; Bondil, M.; Head-Gordon, M.; Bell, A. T. Mechanism and Kinetics of Propane Dehydrogenation and Cracking over Ga/H-MFI Prepared via Vapor-Phase Exchange of H-MFI with GaCl3. *J. Am. Chem. Soc.* **2019**, *141* (4), 1614−1627.
(57) Vityuk, A.; Khivantsev, K.; Aleksandrov, H. A.; Vayssilov, G. N.; Alexeev, O. S.; Amiridis, M. D. Room-Temperature Ethene Hydrogenation Activity of Transition-Metal-Free HY Zeolites. *ACS Catal.* **2019**, *9* (2), 839−847.
(58) Wu, D.; Hernández, W. Y.; Zhang, S.; Vovk, E. I.; Zhou, X.; Yang, Y.; Khodakov, A. Y.; Ordomsky, V. V. In Situ Generation of Brønsted Acidity in the Pd-I Bifunctional Catalysts for Selective Reductive Etherification of Carbonyl Compounds under Mild Conditions. *ACS Catal.* **2019**, *9*, 2940−2948.
(59) Fujitani, T.; Nakamura, I.; Akita, T.; Okumura, M.; Haruta, M. Hydrogen Dissociation by Gold Clusters. *Angew. Chem., Int. Ed.* **2009**, *48* (50), 9515−9518.
(60) Powell, C. D.; Daigh, A. W.; Pollock, M. N.; Chandler, B. D.; Pursell, C. J. CO Adsorption on Au/TiO2 Catalysts: Observations, Quantification, and Explanation of a Broad-Band Infrared Signal. *J. Phys. Chem. C* **2017**, *121* (44), 24541−24547.
(61) Pollock, M. N.; Peterson, C.; Pursell, C.; Chandler, B. D. In *Gold nanoparticle catalysts: Chemical properties and catalytic behavior*; American Chemical Society: 2017.
(62) Panayotov, D. A.; Yates, J. T. Spectroscopic Detection of Hydrogen Atom Spillover from Au Nanoparticles Supported on TiO2: Use of Conduction Band Electrons. *J. Phys. Chem. C* **2007**, *111* (7), 2959−2964.
(63) Powell, C. D.; Daigh, A. W.; Pollock, M. N.; Chandler, B. D.; Pursell, C. J. CO Adsorption on Au/TiO2 Catalysts: Observations, Quantification, and Explanation of a Broad-Band Infrared Signal. *J. Phys. Chem. C* **2017**, *121* (44), 24541−24547.
(64) Panayotov, D. A.; Burrows, S. P.; Yates, J. T.; Morris, J. R. Mechanistic Studies of Hydrogen Dissociation and Spillover on Au/TiO2: IR Spectroscopy of Coadsorbed CO and H-Donated Electrons. *J. Phys. Chem. C* **2011**, *115* (45), 22400−22408.
(65) Prins, R. Hydrogen Spillover. Facts and Fiction. *Chem. Rev.* **2012**, *112* (5), 2714−2738.
(66) Berger, T.; Sterrer, M.; Diwald, O.; Knoezinger, E.; Panayotov, D.; Thompson, T. L.; Yates, J. T., Jr. Light-Induced Charge Separation in Anatase TiO2 Particles. *J. Phys. Chem. B* **2005**, *109* (13), 6061−6068.
(67) Widmann, D.; Krautsieder, A.; Walter, P.; Brueckner, A.; Behm, R. J. How Temperature Affects the Mechanism of CO Oxidation on Au/TiO2: A Combined EPR and TAP Reactor Study of the Reactive Removal of TiO2 Surface Lattice Oxygen in Au/TiO2 by CO. *ACS Catal.* **2016**, *6* (8), 5005−5011.
(68) Widmann, D.; Hocking, E.; Behm, R. J. On the origin of the selectivity in the preferential CO oxidation on Au/TiO2 - Nature of the active oxygen species for H2 oxidation. *J. Catal.* **2014**, *317*, 272−276.
(69) Widmann, D.; Behm, R. J. Activation of Molecular Oxygen and the Nature of the Active Oxygen Species for CO Oxidation on Oxide Supported Au Catalysts. *Acc. Chem. Res.* **2014**, *47* (3), 740−749.
(70) Kumar, G.; Tibbitts, L.; Newell, J.; Panthi, B.; Mukhopadhyay, A.; Rioux, R. M.; Pursell, C. J.; Janik, M.; Chandler, B. D. Evaluating differences in the active-site electronics of supported Au nanoparticle catalysts using Hammett and DFT studies. *Nat. Chem.* **2018**, *10*, 268.
(71) Segura, Y.; Lopez, N.; Perez-Ramirez, J. Origin of the superior hydrogenation selectivity of gold nanoparticles in alkyne + alkene mixtures: Triple- versus double-bond activation. *J. Catal.* **2007**, *247* (2), 383−386.
(72) Nikolaev, S. A.; Smirnov, V. V. Synergistic and size effects in selective hydrogenation of alkynes on gold nanocomposites. *Catal. Today* **2009**, *147*, S336−S341.
(73) Bruno, J. E.; Sravan Kumar, K. B.; Dwarica, N. S.; Hüther, A.; Chen, Z.; Guzman IV, C. S.; Hand, E. R.; Moore, W. C.; Rioux, R. M.; Grabow, L. C.; Chandler, B. D. On the Limited Role of Electronic Support Effects in Selective Alkyne Hydrogenation: A Kinetic Study of Au/MOx Catalysts Prepared from Oleylamine-Capped Colloidal Nanoparticles. *ChemCatChem* **2019**, *11* (6), 1650−1664.
(74) Jenkins, A. H.; Musgrave, C. B.; Medlin, J. W. Enhancing Au/TiO2 Catalyst Thermostability and Coking Resistance with Alkyl Phosphonic-Acid Self-Assembled Monolayers. *ACS Appl. Mater. Interfaces* **2019**, *11* (44), 41289−41296.
(75) Luneau, M.; Shirman, T.; Foucher, A. C.; Duanmu, K.; Verbart, D. M. A.; Sautet, P.; Stach, E. A.; Aizenberg, J.; Madix, R. J.; Friend, C. M. Achieving High Selectivity for Alkyne Hydrogenation at High Conversions with Compositionally Optimized PdAu Nanoparticle Catalysts in Raspberry Colloid-Templated SiO2. *ACS Catal.* **2020**, *10* (1), 441−450.
(76) Hugon, A.; Delannoy, L.; Louis, C. Influence of the reactant concentration in selective hydrogenation of 1,3-butadiene over supported gold catalysts under alkene rich conditions: a consideration of reaction mechanism. *Gold Bull. (London, U. K.)* **2009**, *42*, 310−320.
(77) Hugon, A.; Delannoy, L.; Krafft, J.-M.; Louis, C. Selective Hydrogenation of 1,3-Butadiene in the Presence of an Excess of Alkenes over Supported Bimetallic Gold-Palladium Catalysts. *J. Phys. Chem. C* **2010**, *114* (24), 10823−10835.
(78) Oakton, E.; Vilé, G.; S. Levine, D.; Zocher, E.; Baudouin, D.; Pérez-Ramírez, J.; Copéret, C. Silver nanoparticles supported on passivated silica: preparation and catalytic performance in alkyne semi-hydrogenation. *Dalton Transactions* **2014**, *43* (40), 15138−15142.
(79) Towns, J.; Cockerill, T.; Dahan, M.; Foster, I.; Gaither, K.; Grimshaw, A.; Hazlewood, V.; Lathrop, S.; Lifka, D.; Peterson, G. D.;

https://dx.doi.org/10.1021/jacs.9b13729
J. Am. Chem. Soc. 2020, 142, 5760−5772

et al. XSEDE: accelerating scientific discovery. *Comput. Sci. Eng.* **2014**, *16* (5), 62−74.

https://dx.doi.org/10.1021/jacs.9b13729
J. Am. Chem. Soc. 2020, 142, 5760−5772